A New Twist in the Photophysics of the GFP Chromophore: A Volume-Conserving Molecular Torsion Couple

Jamie Conyard[1], Ismael A. Heisler[1], Yohan Chan[1], Philip C. Bulman Page[1], Stephen R. Meech[1]* and Lluís Blancafort[2]*

[1]School of Chemistry, University of East Anglia, Norwich Research Park, Norwich NR4 7TJ, UK and [2]Institut de Química Computacional and Departament de Química, Facultat de Ciències, Universitat de Girona, C/ M. A. Capmany 69, 17003 Girona, SPAIN

Electronic Supplementary Information

1. Synthetic methods and characterization

Synthesis of methyl HBDI analogue:

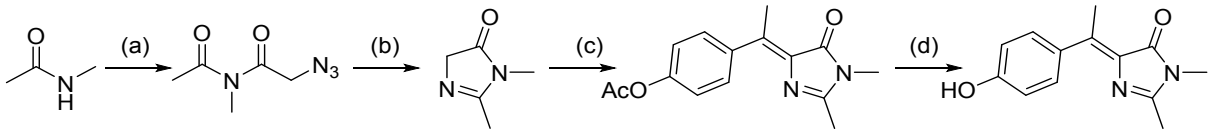

***N*-Acetyl-2-azido-*N*-methylacetamide**:[1]

N-Methylacetamide (7.6 mL, 0.10 mol) and triethylamine (15.2 mL, 0.11 mol, 1.1 equiv.) were dissolved in anhydrous dichloromethane (100 mL) and the reaction mixture was cooled to 0 °C. 2-Chloroacetyl chloride (8.8 mL, 0.11 mol, 1.1 equiv.) was then added dropwise and the reaction mixture was allowed to reach room temperature and was stirred for a further 2 h. Water (30 mL) was then added, and the organic layer was separated. The organic layer was then washed with water (2 x 30 mL), brine (30 mL), dried over anhydrous sodium sulfate and the solvents were removed under reduced pressure. The residue was dissolved in dimethylsulfoxide (100 mL) and sodium azide (13.0 g, 0.20 mmol, 2.0 equiv.) was then added in one portion. The reaction mixture was vigorously stirred overnight at room temperature. The mixture was then poured onto ice-cold water and the solution was then extracted with ethyl acetate (3 x 50 mL). The organic layers were then combined, washed with water (3 x 30 mL), brine (30 mL), dried over anhydrous sodium sulfate and the solvents were removed under reduced pressure. The residue was purified using silica gel flash column chromatography (hexane: ethyl acetate 4:1 to 1:1) to give the desired product as a yellow oil (2.9 g, 19%).

ν_{max} (film)/cm^{-1}: 2106, 1698, 1371, 1308, 1238, 1142, 1064; ^{1}H NMR (500 MHz, $CDCl_3$): δ_H 2.36 (3H, s), 3.28 (3H, s), 4.40 (2H, s); ^{13}C NMR (125 MHz, $CDCl_3$): δ_C 25.7, 32.1, 55.8, 171.4, 173.2.

1,2-Dimethyl-1*H*-imidazol-5(4*H*)-one:[s1]

N-Acetyl-2-azido-*N*-methylacetamide (2.60 g, 0.017 mol) was dissolved in anhydrous toluene (85 mL, 0.2M) and triphenylphosphine (4.80 g, 0.018 mol, 1.1 equiv.) was added in one portion. The reaction mixture was allowed to stir at room temperature overnight. The solvent was removed under reduced pressure and the residue was purified using silica gel flash column chromatography (ethyl acetate: methanol 95:5 to 90:10) to give the desired product as a yellow oil (1.70 g, 91%).

ν_{max} (film)/cm^{-1}: 1726, 1638, 1426, 1397, 1364, 1325, 1167, 973. ^{1}H NMR (500 MHz, $CDCl_3$): δ_H 2.21 (3H, t, J = 2 Hz), 3.07 (3H, s), 4.05 (2H, q, J = 2 Hz); ^{13}C NMR (125 MHz, $CDCl_3$): δ_C 16.1, 26.6, 58.6, 163.3, 181.4.

4-Acetoxy acetophenone:[s2]

Acetophenone (10.0 g, 0.07 mmol) and triethylamine (14.3 mL, 0.10 mol, 1.4 equiv.) were dissolved in anhydrous tetrahydrofuran (100 mL). The solution was cooled to 0 °C and acetyl chloride (6.3 mL, 0.09 mol, 1.2 equiv.) was added slowly. The reaction mixture was allowed to stir overnight at room temperature. The reaction mixture was then filtered on a pad of silica, and ethyl acetate was used to wash the silica. The solvents were evaporated under reduced pressure to yield the desired product as a yellow oil (13.1 g, quant.).

ν_{max} (film)/cm^{-1}: 1760, 1683, 1599, 1359, 1267, 1196, 1164; ^{1}H NMR (500 MHz, $CDCl_3$): δ_H 2.33 (3H, s), 2.60 (3H, s), 7.18-7.21 (2H, m), 7.98-8.01 (2H, m); ^{13}C NMR (125 MHz, $CDCl_3$): δ_C 21.3, 26.7, 121.9, 130.1, 134.9, 169.0, 197.0.

4-Acetoxy-Me-HBDI:

1,2-Dimethyl-1*H*-imidazol-5(4*H*)-one (590 mg, 5.26 mmol, 2 equiv.) and *p*-acetoxy-acetophenone (470 mg, 2.63 mmol) were dissolved in anhydrous tetrahydrofuran and the reaction mixture was cooled to −10 °C. $TiCl_4$ (1.2 mL, 10.52 mmol, 4 equiv.) was added and the mixture was allowed to stir for 40 min at −10 °C. Pyridine (0.85 mL, 10.52 mmol, 4 equiv.) was added over a 30 min period and the reaction mixture was allowed to stir for 2 h at −10 °C and overnight at room temperature. Saturated aqueous ammonium chloride (5 mL) was added and the reaction mixture was evaporated under reduced pressure. The residue was extracted with ethyl acetate (3x20 mL). The organic layers were combined, washed with brine, dried over anhydrous sodium sulphate, filtered and concentrated under reduced pressure. The residue was purified using silica gel flash column chromatography (dichloromethane: methanol 95:5) to give the desired product as a yellow foam (125 mg, 17%).

ν_{max} (film)/cm^{-1}: 1754, 1697, 1631, 1368, 1199, 1169, 1015, 913. ^{1}H NMR (500 MHz, $CDCl_3$): δ_H 2.27 (3H, s), 2.31 (3H, s), 2.74 (3H, s), 3.16 (3H, s), 7.11-7.15 (2H, m), 7.74-7.78 (2H, m). ^{13}C NMR (125 MHz, $CDCl_3$): δ_C 16.5, 18.2, 21.3, 26.6, 121.2, 131.2, 136.3, 137.6, 143.9, 151.1, 158.7, 169.3, 170.1; HRMS (nano-electrospray) *m/z* found for $[M+H]^+$ 273.1234; $[C_{15}H_{16}N_2O_3+H]^+$ requires 273.1234.

I:

p-Acetoxy-Me-HBDI (80 mg, 0.29 mmol) was dissolved in anhydrous dichloromethane (5 mL). Piperidine (60 µL, 0.58 mmol, 2 equiv.) was added and the reaction was allowed to stir for 3 h.

Saturated aqueous ammonium chloride (5 mL) was added and the reaction mixture was extracted with ethyl acetate (2x10 mL). The organic layers were combined, washed with brine, dried over anhydrous sodium sulphate, filtered and concentrated under reduced pressure. The residue was purified using silica gel flash column chromatography (dichloromethane: methanol 9:1) to give the desired product as a yellow foam (62 mg, 93%).

ν_{max} (film)/cm^{-1}: 3276, 1686, 1605, 1511, 1443, 1273, 1177, 838, 735. ^{1}H NMR (500 MHz, $CDCl_3$): δ_H 2.33 (3H, s), 2.71, (3H, s), 3.19 (3H, s), 6.52-6.56 (2H, m), 7.32-7.36 (2H, m); ^{13}C NMR (125 MHz, $CDCl_3$): δ_C 14.8, 19.0, 26.5, 115.9, 130.8, 134.3, 134.1, 148.2, 158.3, 158.4, 169.2; HRMS (nano-electrospray) *m/z* found for $[M+H]^+$ 231.1127; $[C_{13}H_{14}N_2O_2+H]^+$ requires 231.1128.

Figure S1. NMR Data.

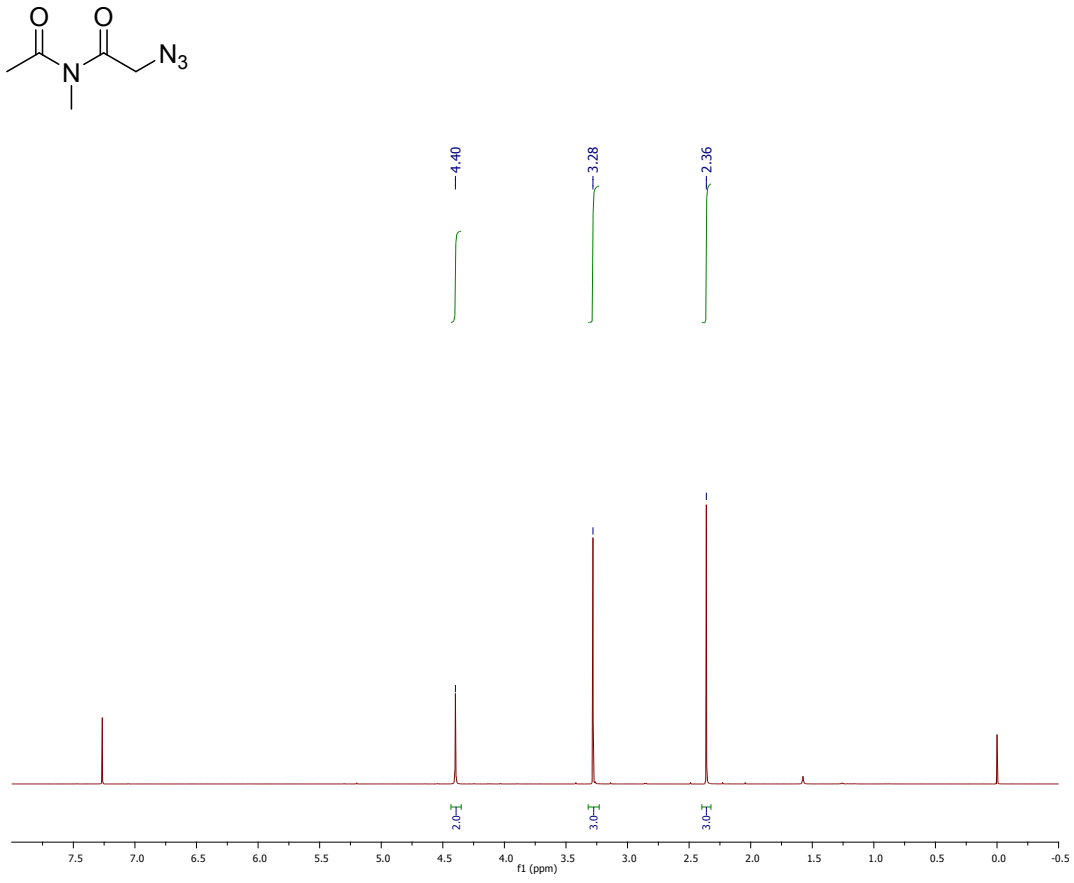

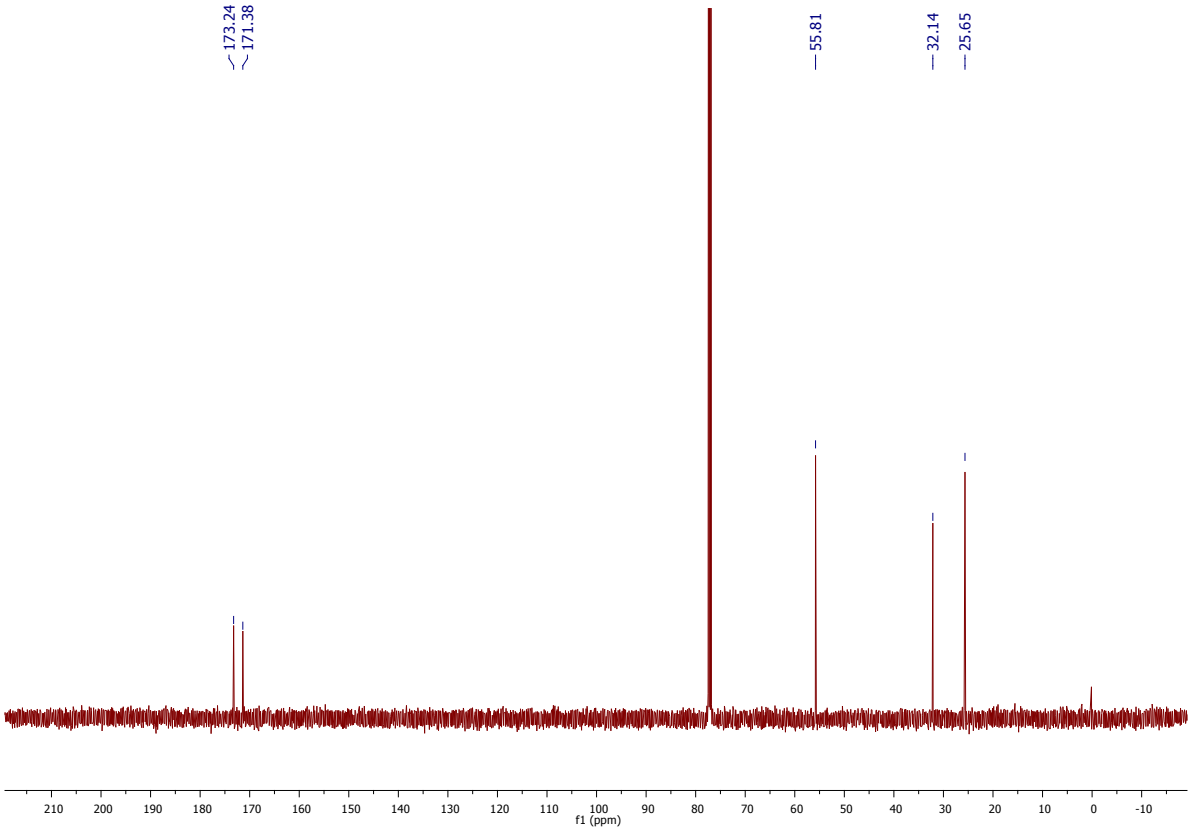
173.24
171.38
55.81
32.14
25.65
210
200
190
180
170
160
150
140
130
120
110
100
90
80
70
60
50
40
30
20
10
0
-10
f1 (ppm)

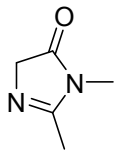
O
N
N

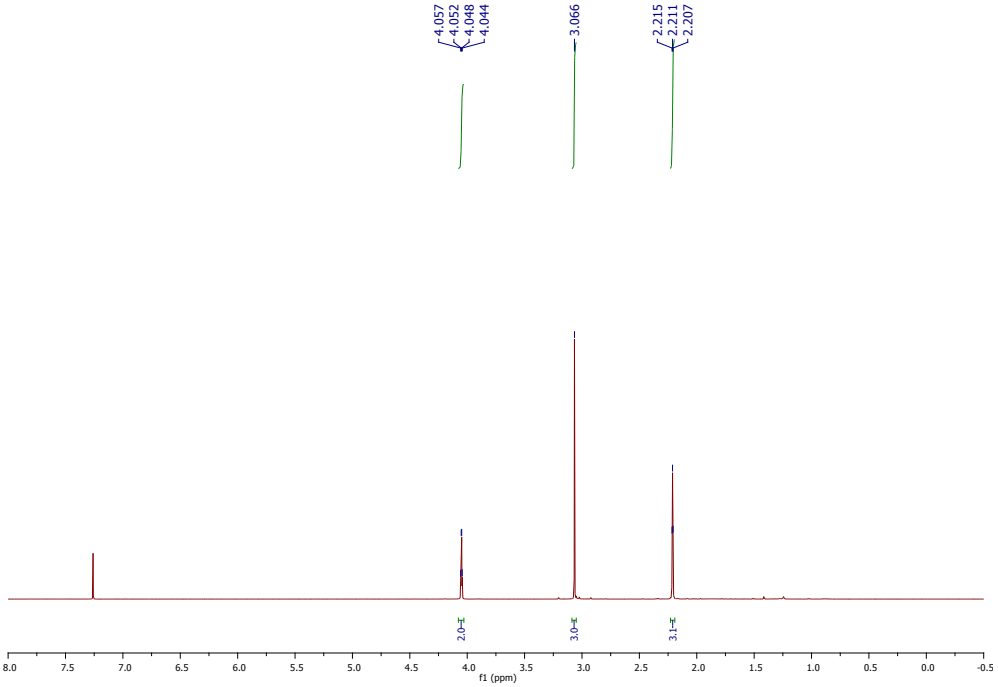
4.057
4.052
4.048
4.044
3.066
2.215
2.211
2.207
2.0
3.0
3.1
f1 (ppm)

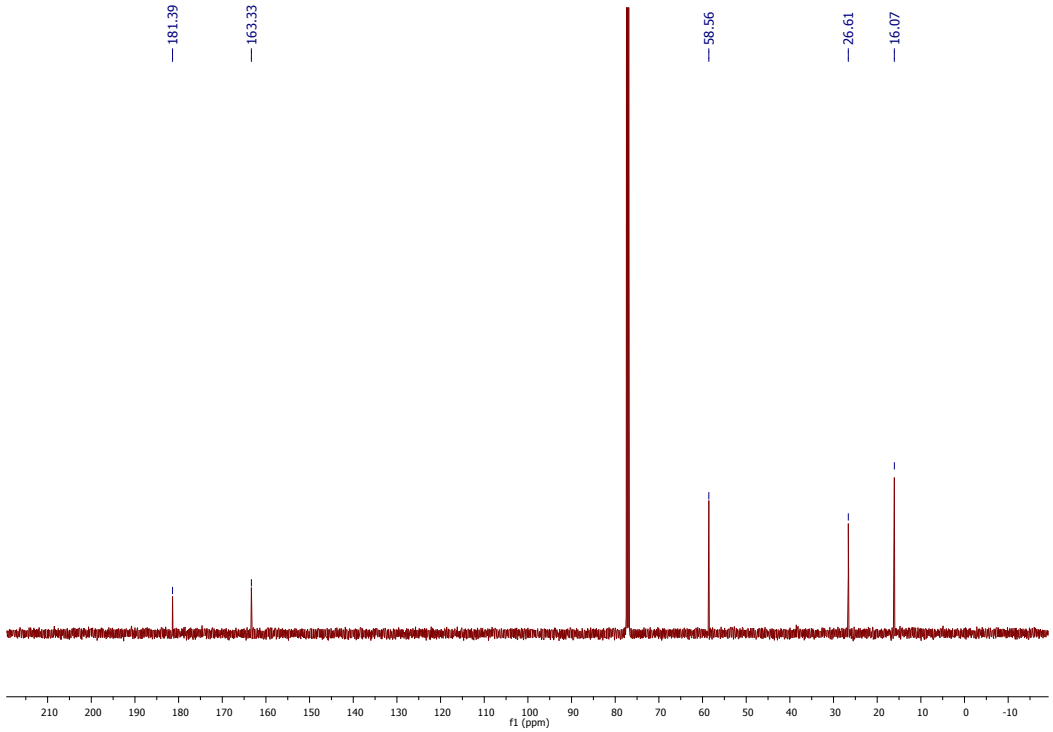
181.39
163.33
58.56
26.61
16.07
f1 (ppm)

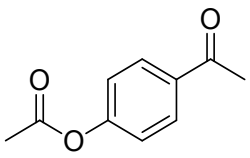
O
O
O

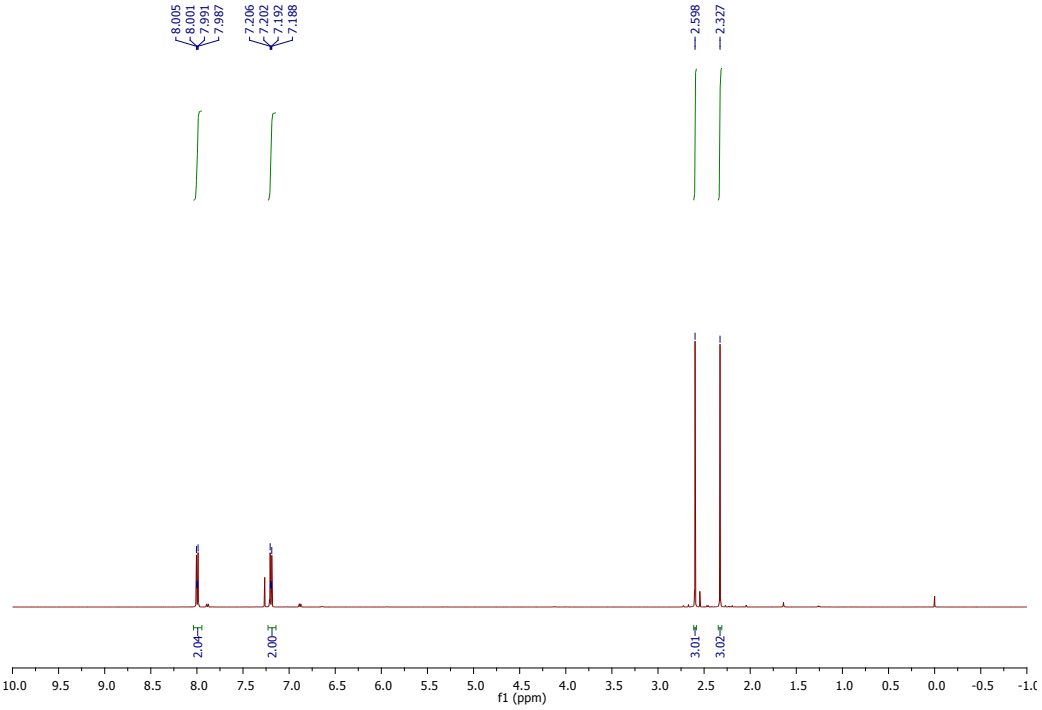
8.005
8.001
7.991
7.987
7.206
7.202
7.192
7.188
2.598
2.327
2.04
2.00
3.01
3.02
f1 (ppm)

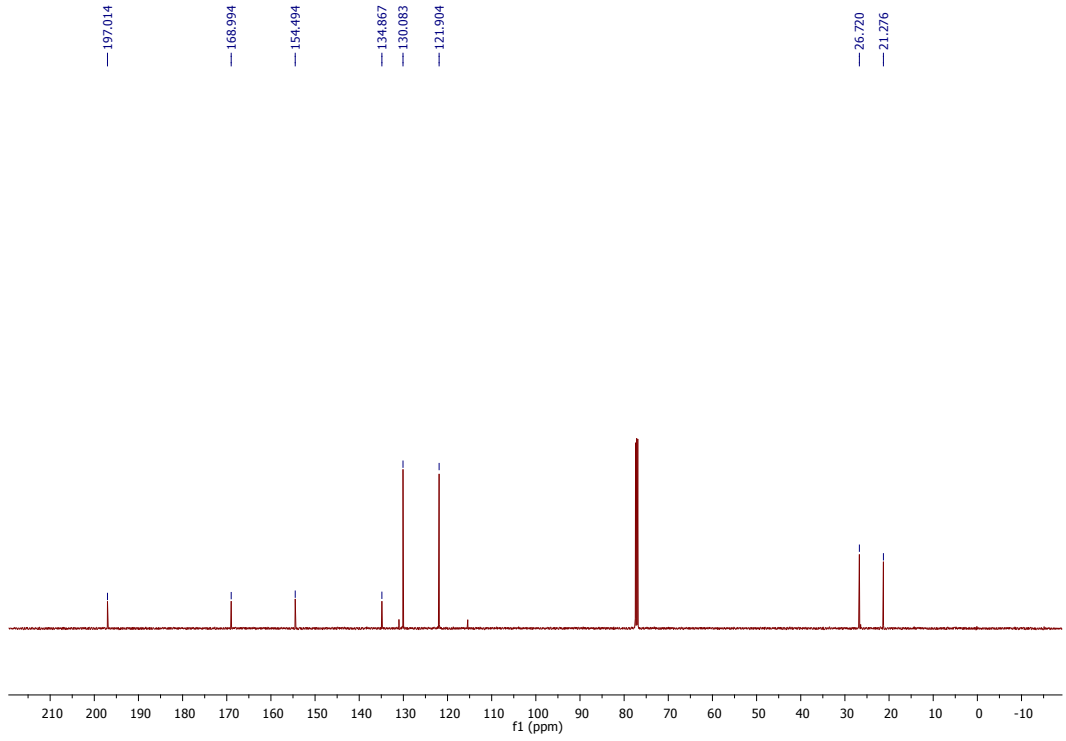
197.014
168.994
154.494
134.867
130.083
121.904
26.720
21.276
f1 (ppm)

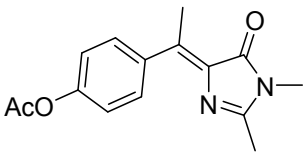
O
N
N
AcO

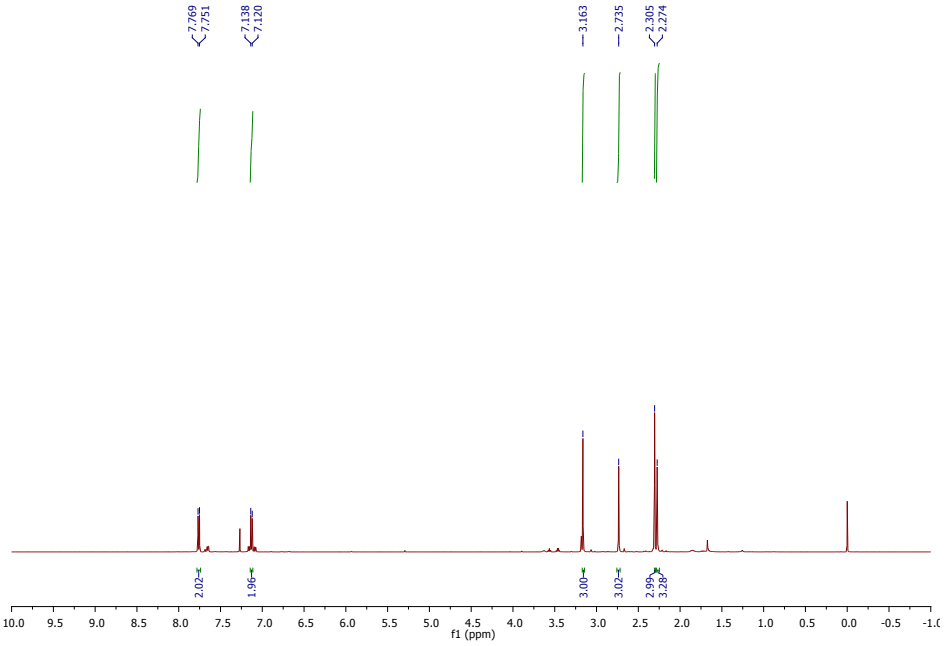
7.769
7.751
7.138
7.120
3.163
2.735
2.305
2.274
2.02
1.96
3.00
3.02
2.99
3.28
f1 (ppm)

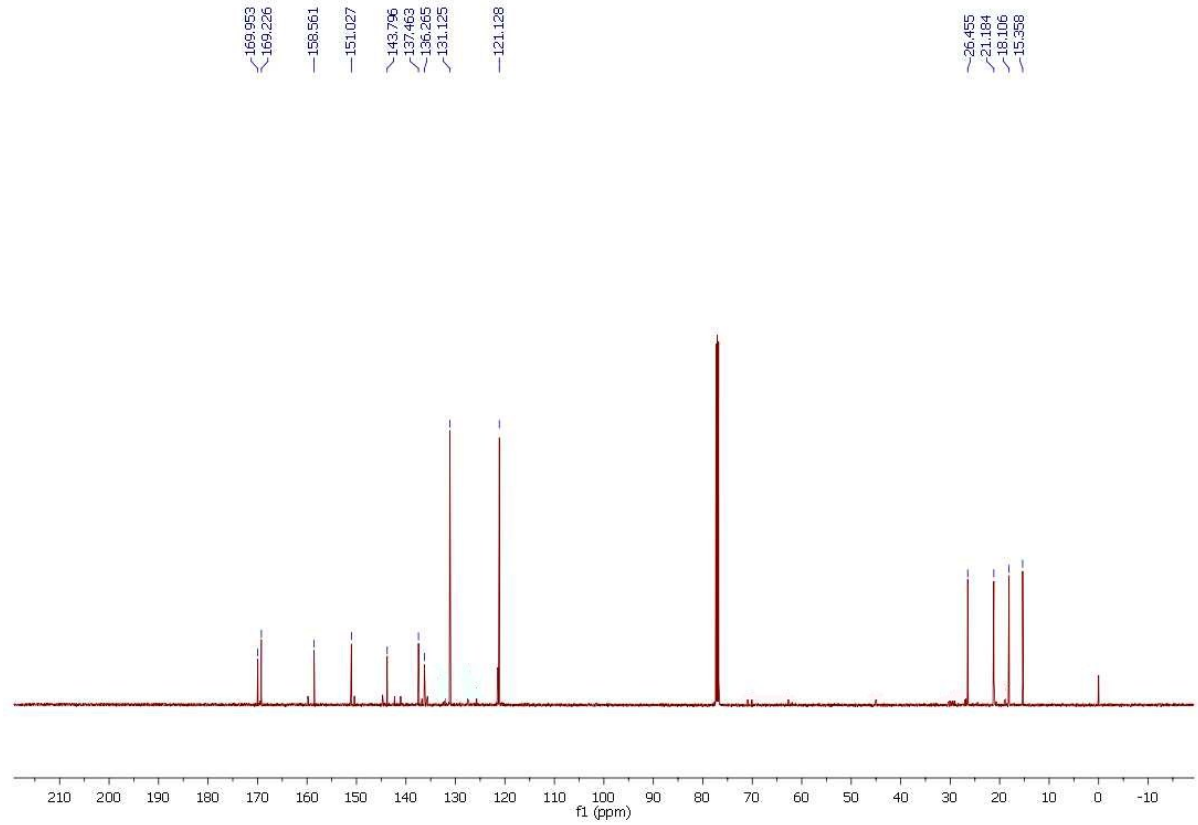
169.953
169.226
158.561
151.027
143.796
137.463
136.265
131.125
121.128
26.455
21.184
18.106
15.358
f1 (ppm)

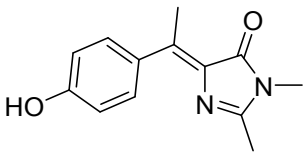
HO
N
N
O

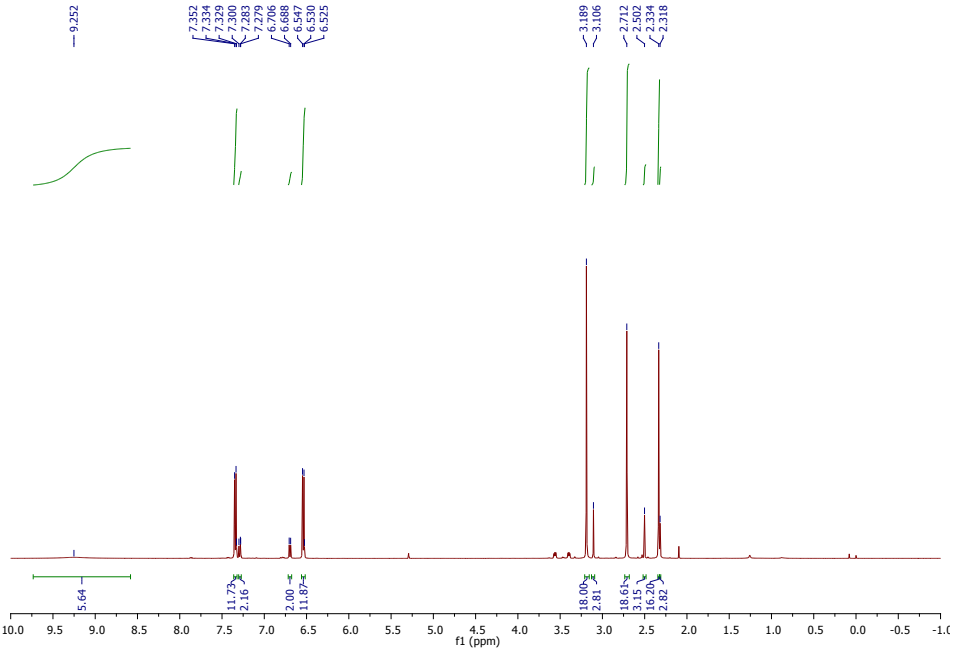
9.252
7.352
7.334
7.329
7.300
7.283
7.279
6.706
6.688
6.547
6.530
6.525
3.189
3.106
2.712
2.502
2.334
2.318
5.64
11.73
2.16
2.00
11.87
18.00
2.81
18.61
3.15
16.20
2.82
f1 (ppm)

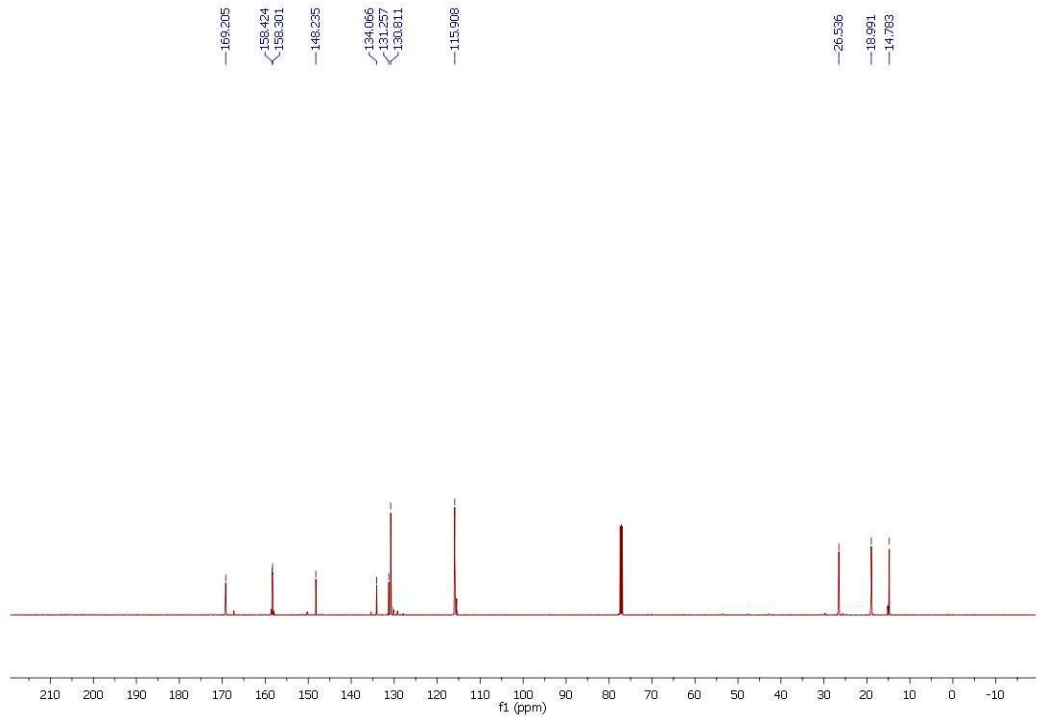
169.205
158.424
158.301
148.235
134.066
131.257
130.811
115.908
26.536
18.991
14.783
f1 (ppm)

2. Fluorescence up-conversion

Fluorescence up-conversion is a variant of the ultrafast pump-probe methods. In our experiment a Ti:sapphire oscillator produces pulses centred at 800 nm of width 20 fs at a 76 MHz repetition rate and a total power of 800 mW. The laser output was compressed by a prism pair and focussed onto a 50 μm thick Type I BBO crystal to produce up to 15 mW of a 400nm second harmonic pump beam. The gate (800 nm) and pump (400 nm) beams were separated with a dichroic mirror, after which they follow different paths, with a temporal separation controlled by a mechanical delay stage which yields and an accuracy in time separation of ca 1 fs. A pair of chirped mirrors was introduced into each beam to compensate for the dispersion introduced by transmission through other optics. The 400 nm pump beam was adjusted to have approx. 8 mW power and was focused with a 150 mm concave mirror to the centre of a 1 mm pathlength cell which contained the sample, which had an optical density of 0.7. The fluorescence emitted from the sample was collected by a reflective microscope objective and focused onto a 100 μm thick Type I BBO crystal where it was mixed with the 800 nm gate beam. A monochromator combined with a photon-counting photomultiplier tube was used to detect the signal generated with a resolution of 15 nm. The intensity of the up-converted signal, at the wavelength selected by the monochromator and the angle of the up-conversion crystal, is proportional to the instantaneous fluorescence intensity during the 20 fs gate pulse, the arrival time of which can be varied by the delay stage. Thus fluorescence up-conversion is an ultrafast sampling technique. The time resolution, measured experimentally by up-converting scattered Raman from the solvent, was determined to be 50 fs and was used in the deconvolution analysis. The apparatus was described in detail elsewhere.[s3]

3. Additional Computational Details.

The energy difference between the *Z*-**I** and *E*-**I** ground-state structures was calculated at the MP2/cc-pvtz, including solvation effects (methanol) with the polarizable continuum model using the integral equation formalism variant[s4a] and adding the zero-point energy correction.

The ground state TS for thermal $Z \longrightarrow E$ isomerization was optimized at the CASSCF/6-311G** level because attempts to optimize it with single-reference methods (MP2 and CAM-B3LYP) failed. The active spaces were 14 electrons in 13 orbitals for MeHBDI and 12 electrons in 12 orbitals for HBDI, and the energy was recomputed with MS-CASPT2 to account for dynamic correlation.

For the TD-CAM-B3LYP/6-311g**decay path optimizations we considered the use of Grimme's empirical correction of the dispersion energy[s4b] and recalculated the initial part of the *Z*-**I** decay path (0 - 8 a.u. of displacement) including the correction in the optimization. The differences between the paths calculated with and without the correction were of the order of only 0.001 Å (bond lenghts), 0.1° (dihedral angles) and 0.01 eV (energies), and the use of the dispersion correction was discarded.

For the MS-CASPT2 calculations we used the ANO-S basis set contracted to 3s2p1d for C, N and O and 2s1p for H and a (16,14) active space which includes 13 π orbitals and the imidazole oxygen lone pair (see Figure S2). 5 states averaged with equal weights were included in the CASSCF and multi-state procedures. The oscillator strength was calculated with the perturbationally modified complete active space configuration interaction wave function and the MS-CASPT2 energies. Cholesky decomposition[s5] with a threshold of 1e-8 a.u. was applied in the calculation of the two-electron integrals, and an imaginary level shift[s6] of 0.1 a.u. and an IPEA shift[s7] of 0.25 a.u were used in the CASPT2 calculations.

The MS-CASPT2 vertical excitation spectrum of the *E*-C_1 isomer is presented in Table SI1. The MP2 ground-state energy profile and the concerted phenyl group rotation along the methyl rotation coordinate is presented in Figure S3.The oscillator strength and geometric parameters along the decay path are presented in Figures S4, S5, S6 and S7.

Table S1. Vertical excitation spectrum (lowest three states) of *E*-**I** at the MS-CASPT2 level (MP2/cc-pvtz optimized geometry). Energies in eV and oscillator strength in brackets.

State	MS-CASPT2/ANO-S[a]	
	E_{ex} [eV][b]	Character
S_1	3.40 (0.127)	H→L (π,π^*)[c]
S_2	4.36 (0.018)	(n_O,π^*)
S_3	4.64 (0.002)	H→L+1, H-2→L (B_{2u}-like)

[a]Active space (16,14), wave function averaged over five states. [b]Oscillator strength in brackets.

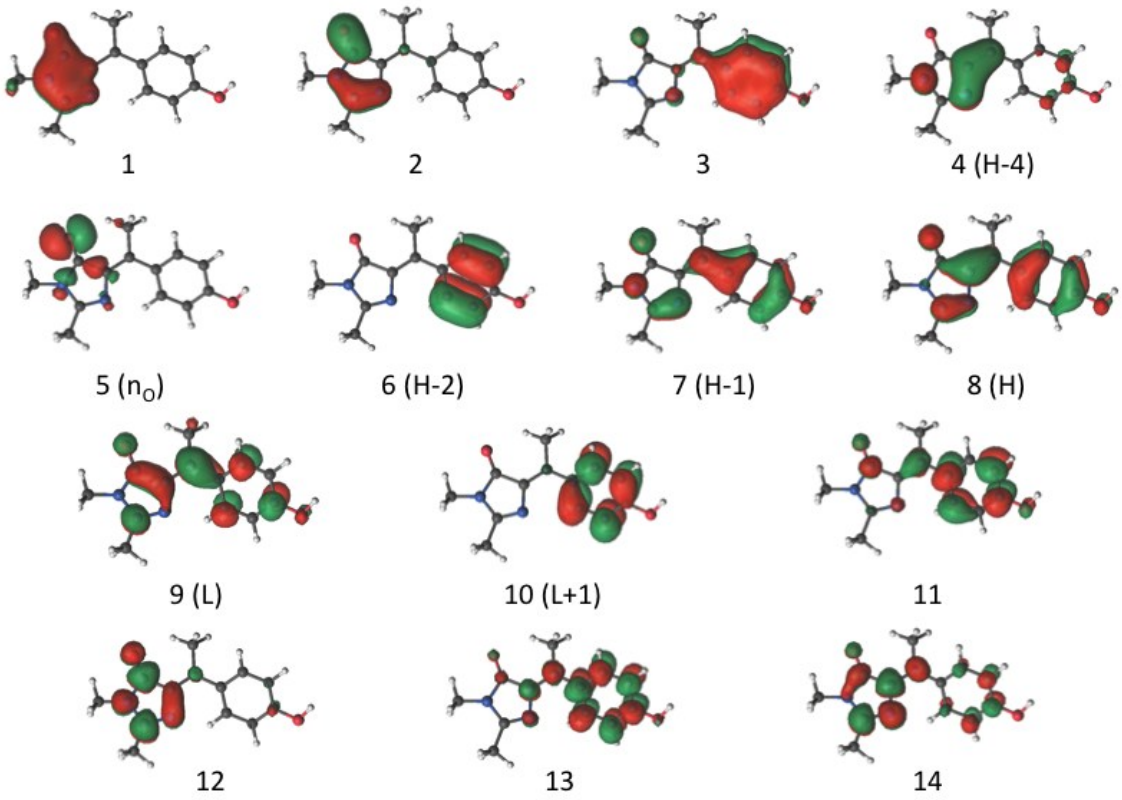

Figure S2. MS-CASPT2 active space for *Z*-**I** at the Franck-Condon geometry. PM-CASCI wave function configuration coefficients: S_1: 0.75 (H⟶L); S_2: 0.78 (n_O⟶L); S_3: 0.48 (H⟶L+1), 0.45 (H-2⟶L); S_4: 0.37 (H-1⟶L); -0.26 (H-4⟶L).

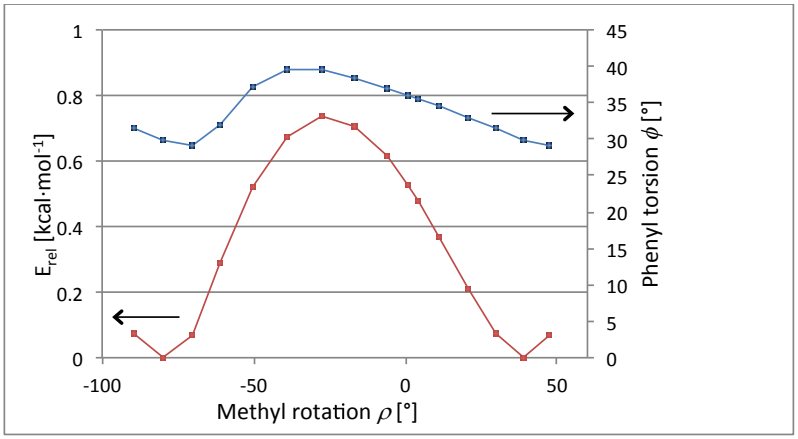

Figure S3. MP2/cc-pvtz ground-state energy profile (brown squares, left *y* axis) and phenyl torsion angle ϕ (blue diamonds, right *y* axis) along the methyl rotation coordinate ρ (see Scheme 1 for a definition) for *Z*-**I**. Structures obtained with a series of ground-state optimizations at fixed values of ρ. Energies relative to the ground-state minimum

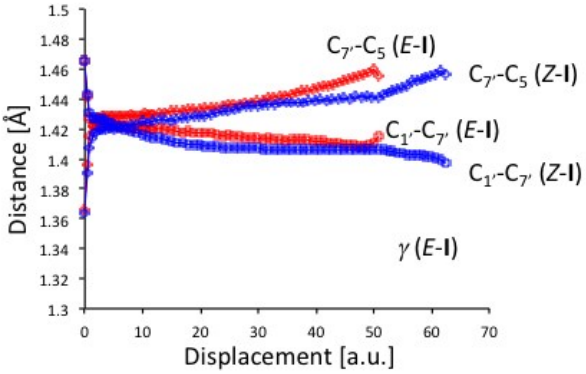

Figure S4. Calculated bond lengths [Å] along the decay path. Blue and red diamonds: $C_{7'}$-C_5 bond for *Z*-**I** and *E*-**I**. Blue and red squares: $C_{1'}$-$C_{7'}$ bond for *Z*-**I** and *E*-**I**.

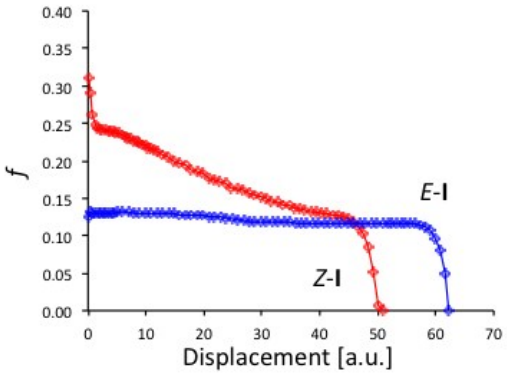

Figure S5. Calculated oscillator strength along the decay path for *Z*-**I** and *E*-**I**.

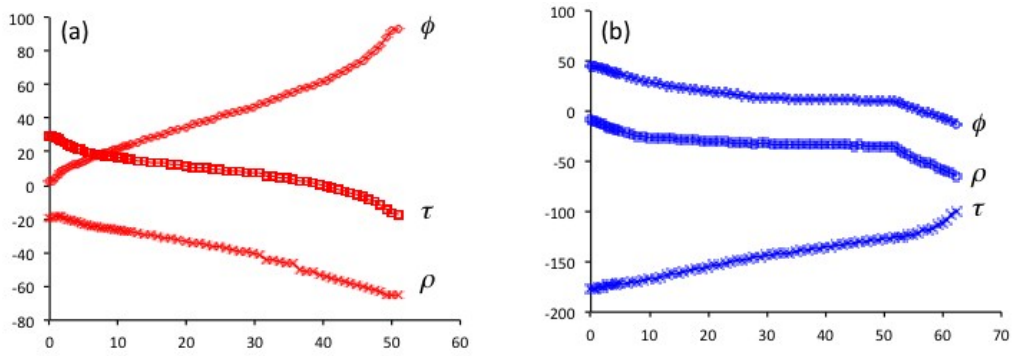

Figure S6. Calculated dihedral angles along the decay path for (a) *Z*-**I** and (b) *E*-**I**. Squares: τ. Diamonds: ϕ. Crosses: ρ. See Scheme 1 for a definition of the angles. Note that changes of ϕ and τ in opposite directions correspond to rotation of the rings in the same direction.

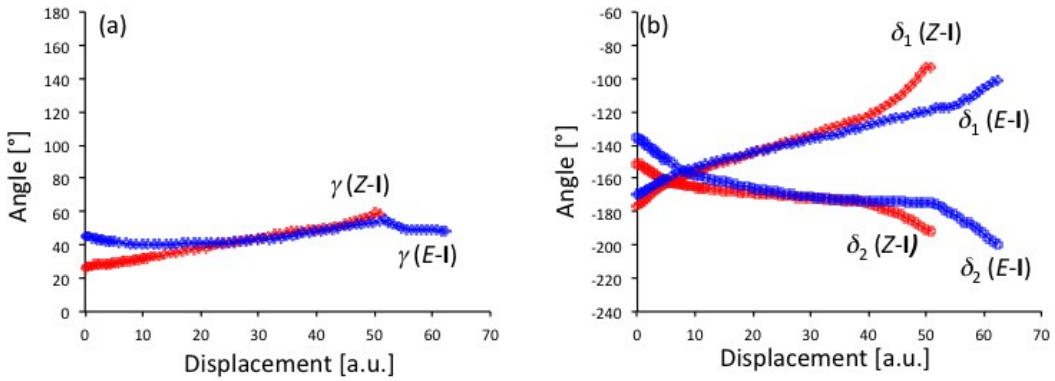

Figure S7. Calculated angles along the decay path for *Z*-**I** (red) and *E*-**I** (blue). (a) Flapping angle γ; (b) Pyramidalization angles δ_1 and δ_2 (diamonds and squares, respectively). δ_1 and δ_2 change by 84° and 40° for *Z*-**I** and by 69° and 64° for *E*-**I**. (c) Illustration of the angles δ_1 and δ_2. Angle definitions (see Scheme 1 for numbering): γ: N_1-C_5-$C_{1'}$-$C_{2'}$ (*Z*-**I**), C_4-C_5-$C_{1'}$-$C_{2'}$ (*E*-**I**); δ_1: C_{Me}-$C_{7'}$-C_5-N_1 (*Z*-**I**), C_{Me}-$C_{7'}$-C_5-C_1 (*E*-**I**); δ_2: C_{Me}-$C_{7'}$-$C_{1'}$-$C_{2'}$ (*Z*-**I** and *E*-**I**).

4.1 Z/E Photoisomerization and Relaxation

Photochemical measurements have shown that irradiation with 365±20 nm light converts Z to E in an analogous fashion to p-HBDI, confirming that Z and E forms have similar spectra. NMR spectra, recorded before and after irradiation, confirmed Z – E isomerisation with no additional photoproducts formed (Figure S8).

Photochemical quantum yields (φ_c: Z→E and φ_t: E→Z) were recovered from photoconversion kinetic measurements according to the method described by Voliani et al.[s8] Briefly, a system undergoing cis-trans isomerisation yields an analytical solution for the time-dependent absorption as follows:

$$A = A^0 + \alpha \cdot A^0 \cdot \varphi_c \cdot (\varepsilon_c - \varepsilon_t) \cdot \frac{(e^{-\lambda t} - 1)}{\lambda} \quad [S1]$$

Where A and A^0 are the total optical density at time *t* and *t*=0, and ε_c and ε_t are the molar extinction coefficients of the Z and E isomers respectively. Two further equations in [S1] are defined:

$$\alpha = \ln 10 \cdot \frac{l \cdot P}{V} \quad [S2]$$

Where *l* is the pathlength, *P* is the power and *V* is the volume of irradiation respectively, and:

$$\lambda = \alpha \cdot (\varepsilon_c \cdot \varphi_c + \varepsilon_t \cdot \varphi_t) \quad [S3]$$

The output of a 365nm lamp (Thorlabs M365LP1) was attenuated to 1 mW and the intensity transmitted through a sample of **I** (2 mL, 0.1 OD, 1 cm pathlength) was recorded as a function of time with a powermeter (Ophir Nova II). The transmitted intensity at time zero (i.e. as soon as the lamp was switched on) was taken as I_0 from which all intensity measurements were converted directly to absorbance (OD). The time domain transmission intensity traces were fit to a single exponential function as follows:

$$F(t) = A_1 e^{\left(-t/\tau_1\right) - 1} + A^0 \quad [S4]$$

This yields a pre-exponential factor:

$$A_1 = \frac{\alpha \cdot A^0 \cdot \varphi_c \cdot (\varepsilon_c - \varepsilon_t)}{\lambda}, \quad [S5]$$

and a time constant:

$$\tau_1 = \frac{1}{\lambda} = \frac{1}{\alpha \cdot (\varepsilon_c \cdot \varphi_c + \varepsilon_t \cdot \varphi_t)}. \qquad [S6]$$

Thus, by determining the molar extinction coefficients of the pure Z (ε_c) and E (ε_t) isomers, the photochemical quantum yields for the Z→E (φ_c) and E→Z (φ_t) processes could be determined directly from the exponential function fit to the time domain intensity data. Beer-Lambert analysis recovered a value of 14000 M^{-1} cm^{-1} for ε_c, whilst ε_t was determined according to the following procedure:

- The absorption spectrum of the pure Z isomer (prepared in the dark) was fit to a log normal function.
- The sample was pumped to the photostationary state with a 365nm lamp and the absorption spectrum was recorded.
- The absorption spectrum of the photostationary state was fit to a function comprising the sum of two log normals. The parameters of the first log-normal function were fixed to those obtained from the log-normal fit to the pure Z isomer (with only the amplitude left as a free fitting parameter). All parameters of the second log-normal function were free fitting parameters.
- The second log normal function was taken as the absorption spectrum of the pure E isomer.
- The integrated intensity of the pure E isomer absorption spectrum was scaled relative to the absorption spectrum of the pure Z isomer in line with the calculated ratio of oscillator strengths (E:Z, 1.5:1).
- The absorption spectra of both the pure Z and E isomers were normalised to a molar extinction coefficient scale using the ε_c value determined experimentally for the Z isomer at 365nm to yield a value of 7800 M^{-1} cm^{-1} for ε_t at 365nm.

The pre-exponent [S5] and time constant [S6] of the exponential function fit to the time-resolved transmitted intensity were then used to calculate φ_c and φ_t directly, the data being reported in the text.

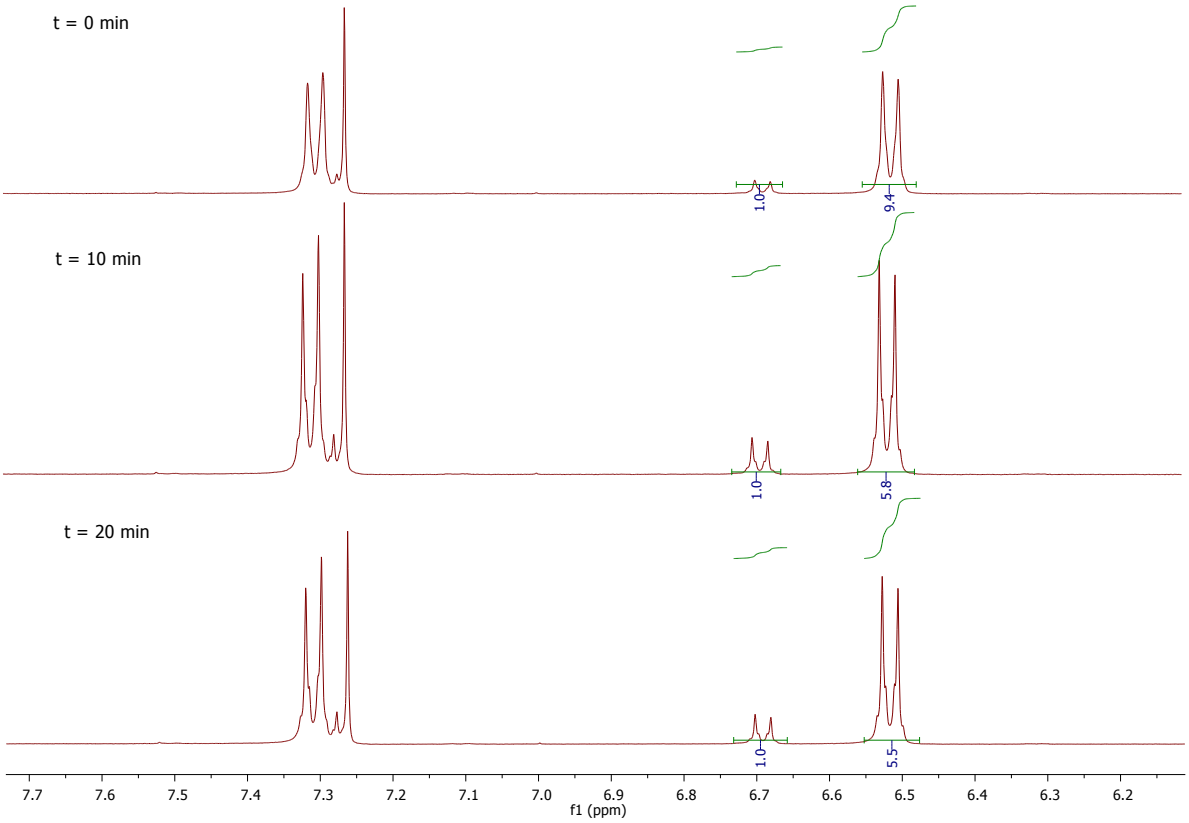

Figure S8. Proton NMR showing formations of the photostationary state after different irradiation times and no additional photoproducts

4.2 Solvent Dependent Recovery from Photostationary State

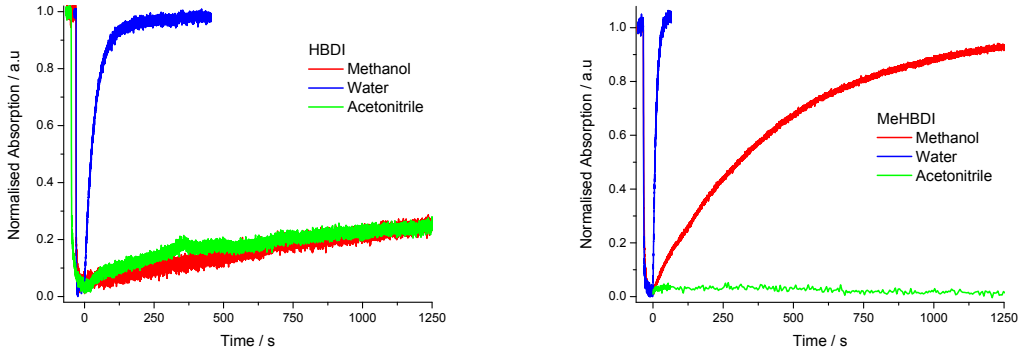

Figure S9 The solvent dependent recovery kinetics for **I** (MeHBDI) and p-HBDI was mentioned in the text. The experimental data is shown here with irradiation stopped at t = 0. The resulting single exponential kinetics were fit and the recovery time is reported below.

solvent	Methanol	Water	Acetonitrile
p-HBDI: τ / s	3159.1	37.4	3554.0
I: τ / s	453.8	11.8	>4000

5. Experimental data for anion of I.

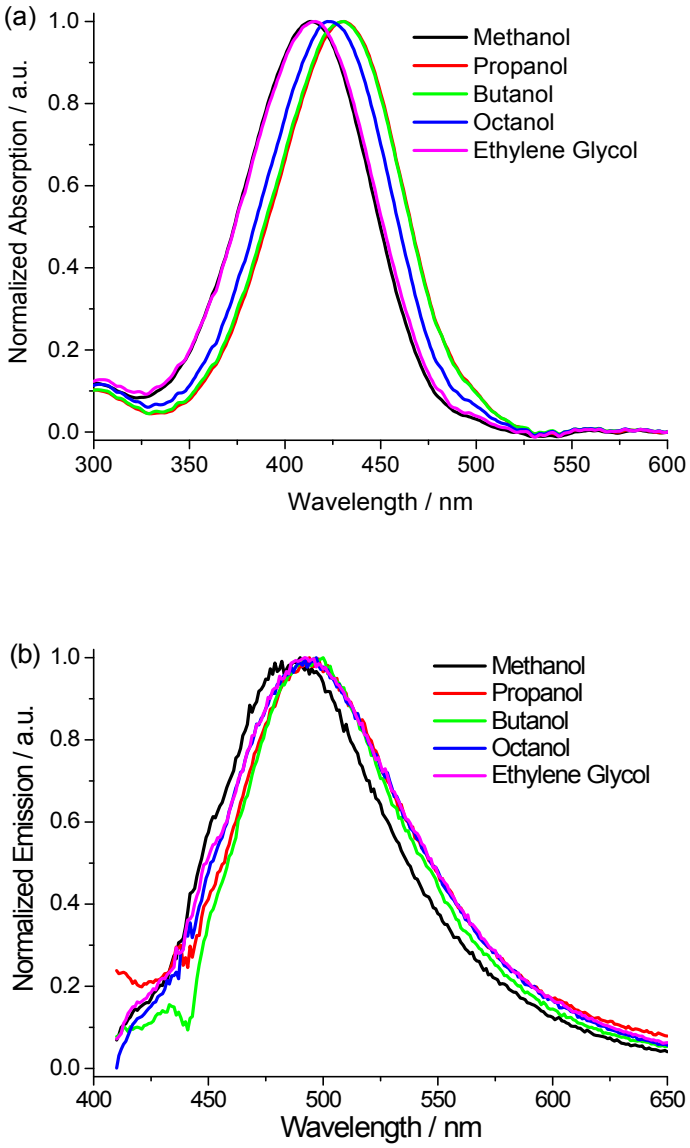

Figure S10. Electronic Spectra, I^-. (a) Electronic absorption spectra and (b) Corresponding emission spectra of the **I** anion in a series of basic alcohol solvents. As for the neutral form, the solvent effect is small.

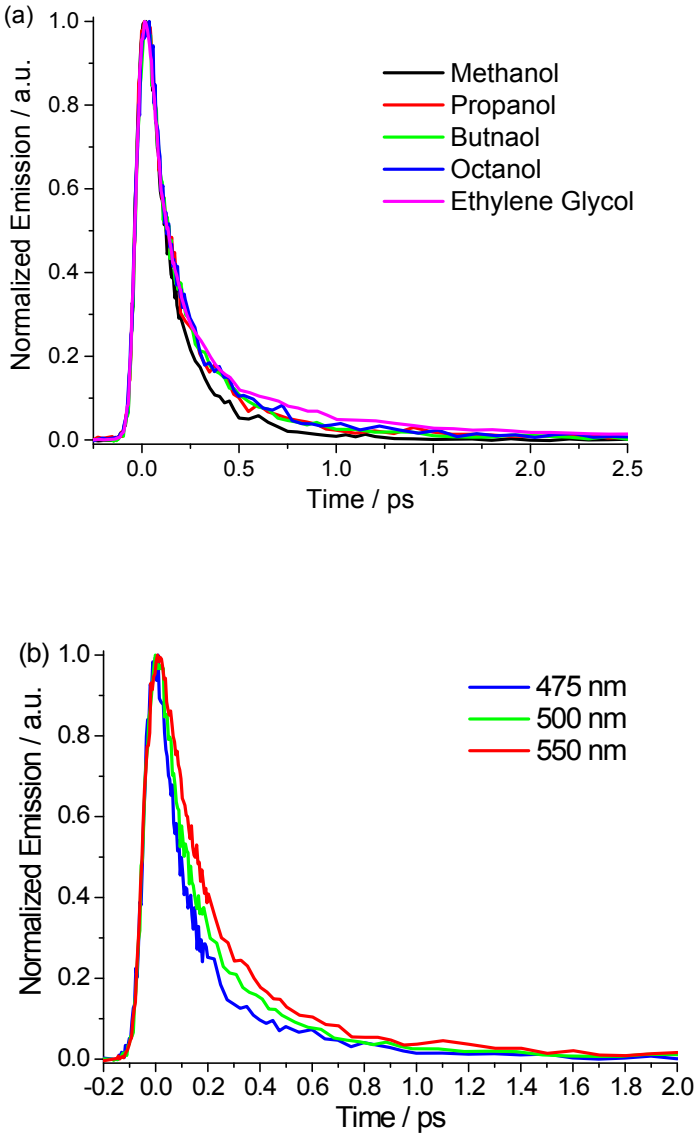

Figure S11. Fluorescence Dynamics of I^-. Time resolved fluorescence decay profiles for the anion of **I** in (a) A selected series of alcohol solvents with emission measured at 500 nm and (b) In butanol as a function of emission wavelength. The negligible viscosity effect and weak wavelength dependence is apparent and similar to the neutral from. The bi-exponential analysis of the data is shown in Table S2

Table S2 Fluorescence decay parameters for I^-. Summary of the exponential parameters of the functions fit to all measured ultrafast fluorescence decay profiles of the anion.

Methanol							
Wavelength / nm	**A_1**	**τ_1 / ps**	**A_2**	**τ_2 / ps**	**A_3**	**τ_3 / ps**	**$\langle\tau\rangle$ / ps**
470	0.71	0.06	0.29	0.20	-	-	0.10
500	0.82	0.10	0.18	0.32	-	-	0.14
550	0.95	0.15	0.05	0.67	-	-	0.18
Propanol							
Wavelength / nm	**A_1**	**τ_1 / ps**	**A_2**	**τ_2 / ps**	**A_3**	**τ_3 / ps**	**$\langle\tau\rangle$ / ps**
470	0.79	0.08	0.21	0.34	-	-	0.13
500	0.74	0.09	0.26	0.38	-	-	0.16
550	0.93	0.17	0.07	1.18	-	-	0.23
Butanol							
Wavelength / nm	**A_1**	**τ_1 / ps**	**A_2**	**τ_2 / ps**	**A_3**	**τ_3 / ps**	**$\langle\tau\rangle$ / ps**
470	0.81	0.09	0.19	0.38	-	-	0.14
500	0.73	0.09	0.27	0.37	-	-	0.17
550	0.89	0.16	0.11	0.78	-	-	0.23
Octanol							
Wavelength / nm	**A_1**	**τ_1 / ps**	**A_2**	**τ_2 / ps**	**A_3**	**τ_3 / ps**	**$\langle\tau\rangle$ / ps**
470	0.81	0.07	0.19	0.39	-	-	0.13
500	0.62	0.06	0.36	0.26	0.02	1.55	0.17
550	0.87	0.17	0.13	0.98	-	-	0.27
Ethylene Glycol							
Wavelength / nm	**A_1**	**τ_1 / ps**	**A_2**	**τ_2 / ps**	**A_3**	**τ_3 / ps**	**$\langle\tau\rangle$ / ps**
470	0.85	0.08	0.15	0.49	-	-	0.14
500	0.57	0.06	0.37	0.23	0.05	1.37	0.19
550	0.86	0.17	0.14	1.35	-	-	0.34

6. Cartesian coordinates of key structures

Z-FC (optimized at MP2/cc-pvtz level of theory)

6	3.791611	0.713853	0.494150
6	2.507717	1.242987	0.446678
6	1.428813	0.499948	-0.059661
6	1.698780	-0.790029	-0.551278
6	2.982502	-1.312559	-0.525223
6	4.035325	-0.567894	0.005314
1	4.604091	1.300842	0.906034
1	2.343907	2.239771	0.830635
1	0.891186	-1.378085	-0.955616
1	3.187646	-2.299458	-0.915838
6	0.094263	1.105462	-0.092596
6	-2.376762	-1.327719	0.144822
6	-1.056294	0.371456	-0.025550
7	-1.110176	-1.022326	0.122700
6	-2.446320	0.912882	-0.077337
8	-2.902823	2.043282	-0.175865
7	-3.222685	-0.242743	0.018088
6	-4.665429	-0.230600	0.030053
1	-4.968127	0.805484	-0.100477
1	-5.068880	-0.828600	-0.784919
1	-5.055902	-0.600854	0.976576
6	-2.910877	-2.702781	0.300096
1	-3.546159	-2.777142	1.183152
1	-3.512128	-2.988153	-0.563669
1	-2.077160	-3.390432	0.399913
6	0.022164	2.603565	-0.173576
1	-0.959452	2.931893	-0.497280
1	0.205353	3.045871	0.808628
1	0.787457	2.980318	-0.850107
8	5.274302	-1.141163	0.011112
1	5.893405	-0.514360	0.400111

E-FC (optimized at MP2/cc-pvtz level of theory)

6	-3.622818	0.592287	-0.757613
6	-2.363447	1.179772	-0.719955
6	-1.338688	0.642168	0.071324
6	-1.633576	-0.479626	0.858953
6	-2.893611	-1.056532	0.843345
6	-3.892318	-0.528229	0.026136
1	-4.396595	1.008784	-1.391627
1	-2.172318	2.048588	-1.334680
1	-0.868580	-0.892193	1.499482
1	-3.120732	-1.916630	1.457090
6	-0.027328	1.294887	0.122425
6	3.291780	0.332599	0.073163
6	1.151441	0.610066	0.118357
7	2.391900	1.259005	0.237075
6	1.376664	-0.843957	-0.138312
8	0.625256	-1.787052	-0.326125
7	2.771391	-0.926169	-0.164852
6	3.486165	-2.157759	-0.395986
1	2.733956	-2.928699	-0.545176
1	4.110102	-2.089424	-1.285407
1	4.105952	-2.421394	0.459436
6	4.756975	0.557046	0.131758
1	5.212476	-0.043568	0.919587
1	5.232319	0.281085	-0.809913
1	4.939995	1.608051	0.331025
6	-0.006966	2.793182	0.177947
1	0.997996	3.155208	0.369725
1	-0.347508	3.209001	-0.772497
1	-0.691151	3.151074	0.947207
8	-5.111693	-1.143094	0.044173
1	-5.693095	-0.673987	-0.563442

Z-CI (last point of TD-DFT MEP calculation)

C	3.859154	0.849287	-0.042756
C	2.632091	1.401998	0.193266
C	1.431190	0.662576	-0.002467
C	1.577714	-0.698557	-0.407067
C	2.814326	-1.241982	-0.690968
C	3.961221	-0.481227	-0.499177
H	4.761211	1.433096	0.107881
H	2.578310	2.433743	0.514256
H	0.689224	-1.311715	-0.417818
H	2.918822	-2.272510	-1.003427
C	0.168923	1.060864	0.497162
C	-2.588472	-1.164535	0.664160
C	-0.983271	0.214517	0.226943
N	-1.407029	-0.775447	1.091549
C	-2.041410	0.598363	-0.647120
O	-2.264972	1.637159	-1.293667
N	-3.066358	-0.333155	-0.288865
C	-4.358808	-0.354439	-0.935010
H	-4.433453	0.566942	-1.511380
H	-4.476827	-1.211468	-1.603484
H	-5.154166	-0.375008	-0.187511
C	-3.245047	-2.438578	1.060062
H	-4.225833	-2.253433	1.510069
H	-3.396283	-3.116652	0.214082
H	-2.618614	-2.936314	1.798253
C	-0.096676	2.332428	1.171072
H	-0.698867	2.846081	0.374625
H	-0.817319	2.221756	1.987249
H	0.759127	2.938826	1.469154
O	5.147901	-1.062944	-0.735486
H	5.867782	-0.451283	-0.549515

E-CI (last point of TD-DFT MEP calculation)

6	-3.756159	0.781654	-0.016988
6	-2.583325	1.468101	-0.111077
6	-1.320100	0.824823	0.076100
6	-1.347623	-0.593102	0.276682
6	-2.541607	-1.272248	0.427708
6	-3.746336	-0.600342	0.276153
1	-4.703796	1.293404	-0.148765
1	-2.617516	2.532756	-0.295900
1	-0.413371	-1.132452	0.266177
1	-2.559241	-2.340436	0.597498
6	-0.104323	1.420674	-0.268584
6	3.095559	0.079891	0.563376
6	1.175683	0.733828	-0.165497
7	2.084199	0.865524	0.859350
6	1.577241	-0.301550	-1.062471
8	0.920139	-0.993606	-1.866335
7	2.815947	-0.712180	-0.503202
6	3.628021	-1.749808	-1.096672
1	2.994850	-2.268024	-1.816254
1	4.504809	-1.347939	-1.611930
1	3.958631	-2.457013	-0.333236
6	4.432683	0.140997	1.210903
1	4.698471	-0.819212	1.665434
1	5.230413	0.401727	0.507446
1	4.401899	0.893268	1.997470
6	0.014926	2.744762	-0.910708
1	0.638746	3.327594	-0.222103
1	0.648181	2.639781	-1.808128
1	-0.911808	3.275455	-1.135958
8	-4.882987	-1.305082	0.392164
1	-5.647571	-0.741602	0.235603

References

S1 Wu, L. X. & Burgess, K. Syntheses of highly fluorescent GFP-Chromophore analogues. *J. Am. Chem. Soc.* **130**, 4089-4096 (2008).

S2 Khersonsky, O. & Tawfik, D. S. Structure-reactivity studies of serum paraoxonase PON1 suggest that its native activity is lactonase. *Biochemistry* **44**, 6371-6382, doi:10.1021/bi047440d (2005).

S3 Heisler, I. A., Kondo, M. & Meech, S. R. Reactive Dynamics in Confined Liquids: Ultrafast Torsional Dynamics of Auramine O in Nanoconfined Water in Aerosol OT Reverse Micelles. *Journal of Physical Chemistry B* **113**, 1623-1631, doi:10.1021/jp808989f (2009).

S4 (a) Cancès, E., Mennucci, B. & Tommasi, J. A new integral equation formalism for the polarizable continuum model: Theoretical background and applications to isotropic and anisotropic dielectrics. *J. Chem. Phys.* **107**, 3032, doi: 10.1063/1.474659 (1997). Cossi, M., Scalmani, G., Rega, N. & Barone, V. New developments in the polarizable continuum model for quantum mechanical and classical calculations on molecules in solution. *J. Chem. Phys.* **117** 43-54, doi: 10.1063/1480445 (2002). (b) Grimme, S., Antony, J., Ehrlich, S. & Krieg, H. A consistent and accurate ab initio parameterization of density functional dispersion correction (DFT-D) for the 94 elements H-Pu. *J. Chem. Phys*. **132**, 154104, doi: 10.1063/1.3382344 (2010).

S5 Pedersen, T. B., Aquilante, F. & Lindh, R. Density fitting with auxiliary basis sets from Cholesky decompositions. *Theor. Chem. Acc.* **124**, 1-10, doi:10.1007/s00214-009-0608-y (2009).

S6 Forsberg, N. & Malmqvist, P. A. Multiconfiguration perturbation theory with imaginary level shift. *Chem. Phys. Lett.* **274**, 196-204, doi:10.1016/s0009-2614(97)00669-6 (1997).

S7 Ghigo, G., Roos, B. O. & Malmqvist, P. A. A modified definition of the zeroth-order Hamiltonian in multiconfigurational perturbation theory (CASPT2). *Chem. Phys. Lett.* **396**, 142-149, doi:10.1016/j.cplett.2004.08.032 (2004).

S8 Voliani, V. *et al.* Cis-trans photoisomerization of fluorescent-protein chromophores. *J. Phys. Chem. B* **112**, 10714-10722, doi:10.1021/jp802419h (2008).